MAPPING FREEZE/THAW BOUNDARIES WITH SMMR DATA

B. W. Zuerndorfer, A. W. England,
M. C. Dobson, and F. T. Ulaby

Radiation Laboratory
Department of Electrical Engineering
and Computer Science
The University of Michigan
Ann Arbor, MI 48109-2122

ABSTRACT

Nimbus 7 SMMR data are used to map daily freeze/thaw patterns in the upper Midwest for the Fall of 1984. The combination of a low 37 GHz radiobrightness and a negative 10.7, 18, and 37 GHz spectral gradient, $\frac{\partial T_b}{\partial f}$, appears to be an effective discriminant for classifying soil as frozen or thawed. The 37 GHz emissivity is less sensitive to soil moisture than are the lower frequency emissivities so that the 37 GHz radiobrightness appears to track soil surface temperature relatively well. The negative gradient for frozen ground is a consequence of volume scatter darkening at shorter microwave wavelengths. This shorter wavelength darkening is not seen in thawed moist soils.

INTRODUCTION

Soil moisture contributes to the energy exchange between the air and ground through latent heats of fusion and vaporization. Whether as boundary conditions for mesoscale climate modelling, or as inputs to an agricultural productivity model, the amount and state of soil moisture are regional parameters that one would like to estimate through satellite remote sensing. There is a large body of literature that addresses the estimation of soil moisture from remotely sensed radiobrightness (e.g. Burke et al., 1979; Wang et al., 1982; Blanchard and Chang, 1983; Schmugge, 1983; Jackson et al., 1984; Camillo and Schmugge, 1984; Schmugge et al., 1986; and Grody, 1988). We present evidence that moisture state can also be inferred from radiobrightness.

Freezing influences the measured radiobrightness temperature of the ground, T_b, through parameters in the approximation (Ulaby et al., 1981),

$$T_b = e\,T_0 + (1\text{-}e)\,T_{sky},$$

where e and T_0 are the emissivity and surface temperature of the ground, respectively, and T_{sky} is the effective sky brightness. In this approximation, atmospheric transmissivity is ignored. Frozen ground exhibits signatures of (1) lower thermal temperatures, T_0, (2) higher emissivity, e, and, as we will demonstrate, (3) a decrease in brightness temperatures with microwave frequency,

$$\frac{\partial T_b}{\partial f} < 0.$$

Signatures (1) and (2) are frequently ambiguous indicators of frozen ground because the changes in radiobrightness that result from freezing may be either positive or negative, depending upon the soil moisture content. Water molecules in frozen plants and soils are not free to align themselves with microwave electric fields. This constraint upon the rotational freedom of water gives rise to an apparent dryness to microwaves. The consequence is a decrease in the real part of the dielectric constant, ε', and an increase in frozen soil emissivity. For example, the real part of dielectric constants, ε', and corresponding emissivities at nadir, $\varepsilon(0)$, of two, homogeneous, smooth surfaced, 15% moist soils at 10 GHz are (ε' from Hoekstra and Delaney, 1974):

Material	+ 5° C			- 5° C		
	ε'	$\varepsilon(0)$	T_b	ε'	$\varepsilon(0)$	T_b
Goodrich Clay	8.2	0.77	221	4.9	0.86	235
Fairbanks Silt	9.6	0.74	214	4.1	0.89	242

Because of increasing emissivity with frequency, a 10° decrease in the clay and silt soil temperatures, from +5° C to -5° C, would cause an increase in T_b of approximately +14 K and +28 K, respectively. The positive direction of change in T_b with soil freezing will cause confusion in discrimination between moist soils which will appear radiometrically warmer when frozen, and dry soils which undergo little molecular change and will appear radiometrically colder.

The shift in emissivity with freezing is most pronounced at the lower microwave frequencies. At 37 GHz, the effect is reduced but not absent. We observe that the 37 GHz radiobrightness correlates relatively well with air temperature (Figure 1). Since soil surface temperature should follow the air temperature, the 37 GHz radiobrightness can be expected to provide a reasonably reliable estimate of soil surface temperature. However, discrimination based only on the 37 GHz radiobrightness would misclassify too often.

Our data suggest a third signature of frozen soil. Freezing reduces the imaginary part of the dielectric constant, ε'', proportionally more than it does the real part, ε'. The loss tangent, $\tan\delta = \varepsilon''/\varepsilon'$, is a measure of the attenuation per microwave wavelength. Reduced loss tangent, or lower attenuation, means that thermally emitted photons originate deeper within emitting media. That is, the effective depth of emission, z_e, $(1-e^{-1}$ of the emission originates above z_e) becomes a larger fraction of the free-space wavelength, λ_0 (England, 1974, 1975, 1976, and 1977). For example, Goodrich Clay and Fairbanks Silt exhibit an increase of z_e with freezing (dielectric data from Hoekstra and Delaney ,1974) ,

Material	+ 5° C				- 5° C			
	ε'	ε''	$\tan\delta$	z_e	ε'	ε''	$\tan\delta$	z_e
Goodrich Clay	8.2	3.5	0.43	$0.13\,\lambda_0$	4.9	1.0	0.20	$0.36\,\lambda_0$
Fairbanks Silt	9.6	5.0	0.52	$0.10\,\lambda_0$	4.1	0.02	0.005	$15.7\,\lambda_0$

The effective emission depth of moist soils is typically 10% of the free-space wavelength. Frozen soils have effective emission depths that may be 30% or more of free-space wavelength. The effective emission depth of frozen sandy soils, like the Fairbanks Silt, can be several wavelengths. In the more transparent emitting media, particularly in frozen sandy soil or dry snow, the greater average thermal photon path lengths have two effects: a greater likelihood that thermal gradients affect spectral gradients, and a greater opportunity for volume scattering of photons.

Thermally induced spectral gradients occur because longer wavelength photons tend to originate below the optical surface where thermal temperatures may differ by several degrees from surface temperatures. For the lower loss tangents of frozen soil, this difference in average emitting depth is enough to reflect near surface thermal gradients caused by diurnal heating. That is, a

positive thermal gradient, $\partial T_O/\partial z$, where z is depth in the soil, will yield a negative spectral gradient, $\partial T_b/\partial f$, where f is microwave frequency. SMMR data are collected at midnight and noon. In the absence of changing weather conditions, midnight thermal gradients will be positive and noon thermal gradients will be negative (Figure 2) so that midnight spectral gradients will be negative, and noon spectral gradients will be positive. An average +0.2 Kelvin/f(GHz) shift in the spectral gradient is observed between midnight and noon for SMMR radiometric brightnesses (Figure 3). We are developing a computer model of these gradient effects. For now, thermally induced spectral gradients are noise to be filtered out.

The second consequence of soil freezing is a greater opportunity for volume scattering -- particularly at shorter microwave wavelengths. This occurs because of the greater average photon path lengths in frozen soil, and because plants and soil appear increasingly heterogeneous at shorter wavelengths. This "law of darkening" means that, for an isothermal, volume scattering halfspace,

$$\frac{\partial T_b}{\partial f} < 0$$

(England, 1974).

Frozen terrain may also be snow covered. Dry snow is exceedingly transparent to microwaves so that snow exhibits significant of darkening (Figure 4, Edgerton et al., 1971). That is, both frozen soil and snow tend to exhibit negative spectral gradients.

While neither a low 37 GHz radiobrightness nor a negative spectral gradient is solely adequate as a classifier of frozen soils, particularly at the relatively coarse resolutions of the Nimbus-7 SMMR, a discriminant based upon a combination of these signatures offers considerable promise. Our objective under NASA Interdisciplinary Research Program Grant NAG5-852 has been to determine whether such a discriminant is feasible.

RADIOBRIGHTNESS AND GROUND TEMPERATURES, AND THE CLASSIFICATION DISCRIMINANT

Nimbus 7 SMMR (Scanning Multichannel Microwave Radiometer) radiobrightness data at 6.6 GHz, 10.7 GHz, 18 GHz, and 37 GHz were obtained for August 1, 1984, through December 31, 1984, over an area that included North Dakota, about half of each neighboring state, and part of southern Canada (Figures 7-9). We chose this large, relatively uniform area because of the low spatial resolution of the SMMR instruments -- 150 Km at 6.6 GHz, 100 Km at 10.7 GHz, 60 Km at 18 GHz, and 30 Km at 37 GHz, and because of the importance of soil moisture state to this region's hydrologic processes. The data arrived from the National Space Science Data Center (NSSDC) on 21, high density, SMMR Cell Tapes. Such data are referenced to latitude and longitude in a satellite-centered coordinate system. We produced two types of image products: Single-band, radiobrightness images at the intrinsic resolution of each sensor, and (2) composite, multi-band images at a common resolution based upon local area averaging. Each radiobrightness pixel was referenced to latitude-longitude in a Mercator projection by interpolation and resampling the Cell Tape data. We used a bi-cubic approximation of a sinc function (Moik, 1980) for the interpolation. H and V radiobrightnesses were averaged to produce a single brightness for each pixel for each frequency.

In addition to large area images, local area spatial averages of radiobrightness were calculated for each radiobrightness channel at 7 meteorologic sites within our test region--Miles

City, MT; Bismark, Fargo, and Williston, ND; and Abileen, Huron, and Rapid City, SD. A local area is defined as a 150 Km cell centered on the meteorological site (150 Km is the spatial resolution of the 6.6 GHz channel). Air and ground temperature data for the Fall of 1984 were obtained from NOAA's National Climatic Data Center in Asheville, North Carolina. Air temperature measurements were available for noon and midnight at the meteorologic sites (i.e., simultaneously with the satellite pass), but ground temperature measurements were for 7:00 a.m. and 7:00 p.m. EST, and were not co-located with the meteorologic sites. Ground temperatures are measured at 5 cm depths. Diurnal heating will weakly affect 5 cm temperatures so that there will be some differences for the times of the satellite pass.

Local area averages at the meteorologic sites were used to define the preliminary boundaries in our Freeze Indicator discriminant. For example, Figure 1 illustrated the correlation between 37 GHz radiobrightness and reported air temperature. The nominal line in these figures is a single best fit linear regression in the least squares sense of all local area averages. Individual linear fits will differ slightly as shown in Figure 1(a). We used the nominal line in our discriminant for simplicity, but a more sophisticated discriminant might use the actual least squares fit for the local area and for the time of day. The discriminant boundaries in Figures 1(b) and 1(c) are merely estimates based upon the nominal regression and a compromise between midnight and noon air temperatures that would imply frozen soil (the lower boundary) and thawed soil (the upper boundary). Remember that diurnal temperature gradients will generally cause midnight, sub-surface soil temperatures to be warmer than air temperatures, and noon, sub-surface soil temperatures to be colder.

Similarly, local area averages of spectral gradient versus air temperature were the bases for the spectral gradient decision boundaries shown in Figure 3. Note that the midnight freeze boundary in this example is relatively unambiguous, while a more effective noon freeze boundary would be shifted upwards by 0.2 K/GHz. Again, for simplicity in this preliminary study, we used discriminant boundaries that were time and location independent.

Our 2-parameter Freeze Indicator incorporates the single-band, 37 GHz radiobrightness, and a spectral gradient based upon linear regression of 10.7, 18, and 37 GHz radiobrightnesses for each pixel. Based upon the decision boundaries in Figure 1(b) and 1(c), the likelihood of frozen ground in a 37 GHz pixel, p_{37}, is estimated as

$$p_{37} = \begin{cases} 0 & Tb(37) > Tb_{max} \\ \dfrac{Tb_{max} - Tb(37)}{Tb_{max} - Tb_{min}} & Tb_{min} < Tb(37) < Tb_{max} \\ 1 & Tb(37) < Tb_{min} \end{cases}$$

where T_b (37) is the measured 37 GHz radiobrightness, and the preliminary decision boundaries are

$$Tb_{max} = 259 \ K$$

$$Tb_{min} = 247 \ K$$

The likelihood of frozen ground based upon spectral gradient decision boundaries in Figure 3(a) and 3(b) is p_{sg}, and is estimated as

4

$$
p_{sg} = \begin{cases} 0 & \dfrac{\partial Tb}{\partial f} > \left(\dfrac{\partial Tb}{\partial f}\right)_{max} \\[3em] \dfrac{\left(\dfrac{\partial Tb}{\partial f}\right)_{max} - \dfrac{\partial Tb}{\partial f}}{\left(\dfrac{\partial Tb}{\partial f}\right)_{max} - \left(\dfrac{\partial Tb}{\partial f}\right)_{min}} & \left(\dfrac{\partial Tb}{\partial f}\right)_{min} < \dfrac{\partial Tb}{\partial f} < \left(\dfrac{\partial Tb}{\partial f}\right)_{max} \\[3em] 1 & \dfrac{\partial Tb}{\partial f} < \left(\dfrac{\partial Tb}{\partial f}\right)_{min} \end{cases}
$$

where the preliminary decision boundaries are

$$
\left(\frac{\partial Tb}{\partial f}\right)_{max} = 0.3 \text{ K/GHz}
$$

$$
\left(\frac{\partial Tb}{\partial f}\right)_{min} = -0.3 \text{ K/GHz}
$$

These boundaries are preliminary in that they were chosen to yield the fewest misclassifications in plots of the type shown in Figure 5(a) and 5(b). More refined discriminants would incorporate area and time specific decision boundaries. This would be relatively straightforward if there were a higher density of weather stations in the test area. As it is, we believe that diurnal temperature modeling well yield effective time dependent boundaries, and, perhaps, requiring sub-region consistency within a classification will yield improved spatially dependent boundaries. These refinements are to be part of our continuing project. However, it is the basic sparseness and lack of control of air and ground data that should prompt some caution about over-interpreting our results.

Our freeze/thaw discriminant, or Freeze Indicator, is the product of p_{37} and p_{sg}, and is applied at the scale of the 10.7 GHz data. Resolution differences between different frequency channels can produce anomalous composite image results if the data were processed directly at their original scale. To avoid these problems, the resolution of the data from each channel is compensated to the (coarse) resolution of the lowest frequency channel used in estimating spectral gradients (i.e. 10.7 GHz and 100 Km resolution). Under certain constraints upon the classification process, these images can be referenced to the higher resolution, 37 GHz format for better location of freeze/thaw boundaries (Zuerndorfer, et al., 1989). The effort needed to do this would be justified as a part of an improved classification process. Figures 7 through 12 include images of the Freeze Indicator for various times during the test period. Black in these images indicates a high likelihood of frozen ground.

OBSERVATIONS

Figure 6(a) and 6(b) show normalized brightness temperatures for midnight and noon, respectively, in the northern Great Plains during the Fall of 1984. Normalized brightnesses are the average regional brightness at each microwave frequency divided by the average regional air temperature. Normalized brightness thus has the dimension of emissivity. Note that there is little systematic ordering among the 10.7, 18, and 37 GHz normalized brightnesses during August through most of November. However, during the latter half of November through December, the normalized brightnesses at midnight are uniformly ordered, 10.7 GHz brightnesses are high, 18 GHz brightnesses are middle, and 37 GHz brightnesses are low. That is, they exhibit negative average spectral gradients. The noon normalized brightnesses for December exhibit a similar trend, but with exceptions. These are, we believe, illustrations of the law of darkening for frozen soils. Soils at midnight in December for the northern Great Plains are very likely to be frozen.

Performance of the freeze/thaw discriminant is demonstrated in Figures 7-9 where Freeze Indicator (FI) images are compared with ground and air temperature measurements for midnight on 9/20/84, 10/24/84, and 12/9/84. Midnight FI images are shown as better examples of the potential of a freeze discriminant. Noon FI images are generally less consistent with meteorologic reports because of the contribution of the noontime positive diurnal spectral gradient to the negative frozen ground spectral gradient that we discussed in the last section. Areas not covered by the satellite in a particular pass are shown in white. Tables 1-3 are summaries of the meteorologic reports.

On the night of September 20 (Fig. 7), air temperatures throughout the region were near 60° F and had been above freezing for several days. The FI image shows weak, probably false indications of freezing in the prairies of ND, southern Canada, and the rolling glacial terrain east of the Red River Valley in Minnesota. While the dry air of the northern prairies permits nighttime radiation cooling of the ground to temperatures below that of the air, the more likely explanation for the weak freeze indication is short wavelength scattering by the tall prairie grasses in the northern great plains, and by woodland areas in Minnesota. However, there are no strong indications of freezing in the FI image.

On the night of October 24 (Fig. 8), air temperatures hovered about freezing throughout the area, but had been below freezing at Williston for several days, and generally above freezing toward the east (see the temperatures for Fargo, Aberdeen, and Huron in Table 2). The FI image shows a strong freeze indication in northwestern ND which is consistent with the temperature patterns. Similarly, the definite thaw indication along the Red River Valley is consistent with the warmer temperatures reported and the generally more moist soil in the Valley.

On the night of December 9 (Fig. 9), air temperatures were generally below freezing except at Rapid City, SD, and had been below freezing for several days. There was no more than trace snow on the ground anywhere in the region. The FI image shows strong freeze indications throughout most of the region with weaker indications near Rapid City, and in the Aberdeen-Fargo sub-region (Aberdeen is not shown on the December 9 map because its temperature report was missing for that date). Again, the FI image is consistent with the temperature record.

37 GHz radiobrightness and FI image sequences were produced at midnight and noon for six-day periods in September, October, and December (Figures 10-12). SMMR coverage is based on a 48 hour cycle--midnight (0000 local hours on the date shown), noon (1200 hours on the same date), and then midnight again 36 hours later. However, orbit precession causes gaps in the cycle and variations in the coverage footprint. Within these constraints, our objective was to observe, if possible, weather dynamics reflected in the FI images.

The 37 GHz sequence beginning on September 16 (Figure 10 and Table 1) shows the moist area associated with the Missouri River, Sakakawea and Devils Lakes in ND, and the Missouri River and Lake Oahe in SD. Rain during the night of September 21 appears as a regional darkening of the 37 GHz image for midnight on the 22nd. Note that the rain is not picked up in the FI image.

The October sequence (Figure 11) is dominated by a cold front passing through the area from the northwest with rain and snow beginning on October 19. The region is warmer and drier by the 26th. The moisture pattern dominates the 37 GHz image, but only the apparent freeze pattern, which generally lags the cold front, is shown in the FI image. Note that strong freeze indications follow the cold front but weaken in the south with warming on the 26th.

The December sequence (Figure 12) is characterized by cold temperatures and snow from December 2 through December 5, followed by daytime warming into the 40's (and even 58° at Rapid City, SD) by the 9th. The FI images reflect this general coldness, but also show daytime thawing toward the end of the period.

CONCLUSIONS

Freeze Indicator images based upon a preliminary, 2-parameter discriminant--37 GHz radiobrightness and 10.7, 18, and 37 GHz spectral gradient--show relatively good correlation with the expected state of moisture in northern Great Plains soils during the Fall of 1984. The discriminant is preliminary in the sense that both theoretical and experimental work needs to be done to fully exploit the diurnal radiobrightness signatures of frozen soils. The concept underlying the preliminary discriminant is that frozen soil will exhibit volume scatter darkening at shorter microwave wavelengths much like the effect observed in dry snow. Few other phenomena cause negative microwave spectral gradients. However, one such phenomenon is diurnal insolation which should cause negative spectral gradients at midnight, but positive spectral gradients at noon. We are in the process of tayloring our discriminant to allow for these diurnal gradients.

Freeze Indicator images based upon SMMR data effectively map temporal variations in the freeze/thaw pattern for the northern Great Plains at the time scale of days. These patterns are synchronized with weather patterns, but are not identical. We intend to expand our test data set to include several complete seasons. The product would be, in essence, a movie of freeze/thaw patterns as weather fronts sweep through the Great Plains throughout several seasons. The development of these data from SMMR archives should provide one aspect of a meso-scale climatic baseline for the region.

7

REFERENCES

Blanchard, B.J., and A.T.C. Chang, 1983, Estimation of soil moisture from Seasat SAR data, Water Res. Bull. 19, p. 803-810.

Burke, W.J., T. Schmugge, and J.F. Paris, 1979, Comparison of 2.8- and 21-cm microwave radiometer observations over soils with emission model calculations, JGR 84, p. 287-294.

Camillo, P.J., and T.J. Schmugge, 1984, Correlating rainfall with remotely sensed microwave radiation using physically based models, IEEE Trans. on Geosc. and Rem. Sens. GE-22, p. 415-423.

Edgerton, A.T., A. Stogryn, and G. Poe, 1971, Microwave Radiometric Investigations of Snowpacks, Final Rept. 1285R-4 of Contract 14-08-001-11828 between Aerojet-General Corp., El Monte, CA, and the U.S. Geological Survey.

England, A.W., 1974, The effect upon microwave emissivity of volume scattering in snow, in ice, and in frozen soil, Proc. URSI Spec Mtg on Microwave Scattering and Emission from the Earth, Berne, Switzerland, 23-26 Sept., 1974.

England, A.W., 1975, Thermal microwave emission from a scattering layer, JGR 80, p. 4484-4496.

England, A.W., 1976, Relative influence upon microwave emissivity of fine-scale stratigraphy, internal scattering, and dielectric properties, Pageoph 114, p. 287-299.

England, A.W., 1977, Microwave brightness spectra of layered media, Geophysics 42, p. 514-521.

Grody, N.C., 1988, Surface identification using satellite microwave radiometers, IEEE Transactions on Geoscience and Remote Sensing, V. 26, p. 850-859.

Hoekstra, P., and A. Delaney, 1974, Dielectric properties of soils at UHF and microwave frequencies, JGR 79, pp.1699-1708.

Moik, J., 1980, Digital Processing of Remotely Sensed Images, NASA SP-431.

Schmugge, T.J., 1983, Remote sensing of soil moisture: Recent advances, IEEE Trans. on Geosc. and Rem. Sens. GE-21, p. 336-344.

Schmugge, T.J., 1987, Remote sensing applications in hydrology, Rev. Geophys. 25, p. 148-152.

Schmugge, T.J., P.E. O'Neill, and J.R. Wang, 1986, Passive microwave soil moisture research, IEEE Trans. on Geosc. and Rem. Sens. GE-24, p. 12-22.

Ulaby, F.T., R.K. Moore, and A.K. Fung, 1981, Microwave Remote Sensing, Active and Passive, Addison-Wesley, p. 186-255.

Wang, J.R., T.J. Schmugge, W.I. Gould, W.S. Glazar, and J.E. Fuchs, 1982, A multi-frequency radiometric measurement of soil moisture content over bare and vegetated fields, Geophys. Res. Let. 9, p. 416-419.

Watson, K., L.C. Rowan, and T.W. Offield, 1983, Application of thermal modeling in the geologic interpretation of IR images, <u>Remote Sensing</u>, <u>SEG Reprint Series</u>, no. 3, p. 345-369.

Zuerndorfer, B., A.W. England, and G.H. Wakefield, 1989, The radiobrightness of freezing terrain, <u>Proc. of IGARSS '89</u>, Vancouver, B.C., July 10-14, in press.

TABLE 1

Year 1984	Site	Air Temp (°F)		Cloud Cover (x/10)		Precip. (in.)				Snow Pack (in.)
		00	12	00	12	00	12	24h	Rem	24h
9/15	Aberdeen	40	63	2	3	0	0	0		0
	Bismark	39	64	0	0	0	0	0		0
	Fargo	46	63	8	0	0	0	T		0
	Huron	44	64	0	3	0	0	0		0
	Miles City	50	65	2	2	0	0	0		0
	Rapid City	44	63	4	2	0	0	0		0
	Williston	48	60	6	0	0	0	0		0
9/16	Aberdeen	46	65	1	3	0	0	0		0
	Bismark	53	67	0	2	0	0	0		0
	Fargo	47	69	0	0	0	0	0		0
	Huron	50	64	5	10	0	0	0		0
	Miles City	58	74	0	3	-	-	0		0
	Rapid City	52	70	3	6	0	0	0		0
	Williston	55	68	0	3	0	0	0		0
9/17	Aberdeen	57	71	2	8	0	0	0		0
	Bismark	56	83	0	1	0	0	0		0
	Fargo	57	73	0	3	0	0	0		0
	Huron	58	73	10	3	0	0	0		0
	Miles City	61	80	0	0	-	-	0		0
	Rapid City	64	84	0	0	0	0	0		0
	Williston	56	74	0	3	0	0	0		0
9/18	Aberdeen	64	81	0	0	0	0	0		0
	Bismark	57	80	0	0	0	0	0		0
	Fargo	64	81	0	0	0	0	0		0
	Huron	62	84	0	0	0	0	0		0
	Miles City	60	80	0	0	-	-	0		0
	Rapid City	63	90	0	0	0	0	0		0
	Williston	67	73	0	0	0	0	0		0
9/19	Aberdeen	59	84	0	1	0	0	0		0
	Bismark	55	86	0	0	0	0	0		0
	Fargo	65	90	0	0	0	0	0		0
	Huron	68	90	0	0	0	0	0		0
	Miles City	67	76	0	0	-	-	0		0
	Rapid City	60	90	0	0	0	0	0		0
	Williston	57	72	0	0	0	0	0		0
9/20	Aberdeen	62	65	0	9	0	0	0		0
	Bismark	58	63	0	9	0	0	0		0
	Fargo	54	62	0	6	0	0	0		0
	Huron	62	71	0	2	0	0	0		0
	Miles City	63	72	7	2	-	-	T		0
	Rapid City	59	67	2	6	0	0	0		0
	Williston	54	51	8	9	0	.01	0.15	(R)	0
9/21	Aberdeen	59	82	2	2	0	0	0.1		0
	Bismark	58	81	8	7	0	0	0.3	(R)	0
	Fargo	59	77	10	9	0	0	0		0
	Huron	60	83	0	0	0	0	0		0
	Miles City	66	56	10	10	-	-	0.18	(R)	0
	Rapid City	60	83	2	1	0	0	0.07	(R)	0
	Williston	57	54	10	10	.02	.01	0.3	(R)	0
9/22	Aberdeen	61	65	8	2	T	0	T		0
	Bismark	52	60	3	1	0	0	0		0
	Fargo	72	66	9	0	T.	0	0.02		0
	Huron	66	66	10	2	.05	0	.011	(R)	0
	Miles City	46	52	4	6	-	-	0		0
	Rapid City	45	60	3	4	0	0	0		0
	Williston	45	44	10	9	0	0	0		0

TABLE 2

Year 1984	Site	Air Temp (°F)		Cloud Cover (x/10)		Precip. (in.)				Snow Pack (in.)
		00	12	00	12	00	12	24h	Rem	24h
10/19	Aberdeen	37	44	10	8	.01	0	.1	(R)	0
	Bismark	36	40	10	10	0	0	.04	(S)	0
	Fargo	40	38	10	10	.07	0.2	.77	(R)	0
	Huron	38	45	10	7	0.1	0	.01		0
	Miles City	28	39	7	4	-	-	T		0
	Rapid City	26	42	2	7	0	T	T		T
	Williston	27	34	2	10	-	-	.1	(S)	0
10/20	Aberdeen	36	44	-	10	0	0	T		0
	Bismark	35	38	9	10	T	.01	.1	(R)	0
	Fargo	37	42	10	10	T	.01	.12	(R)	0
	Huron	35	41	0	10	0	0	T		0
	Miles City	31	33	10	10	-	-	.01	(S)	0
	Rapid City	26	43	0	0	0	0	T	(S)	0
	Williston	33	33	10	10	.02	0	.08	(S)	T
10/21	Aberdeen	37	41	-	10	0	0	T		0
	Bismark	36	37	10	10	0	0	.03	(S)	0
	Fargo	38	39	10	9	0	T	.07	(R)	0
	Huron	35	44	2	6	0	0	T		0
	Miles City	29	32	8	9	-	-	T		T
	Rapid City	33	38	10	10	T	0	T	(S)	T
	Williston	32	33	10	9	.01	0	T	(S)	T
10/22	Aberdeen	34	41	7	8	0	0	T		T
	Bismark	33	39	10	8	0	0	0		T
	Fargo	36	38	10	10	T	0	T		0
	Huron	31	42	0	3	0	0	0		0
	Miles City	25	38	0	7	-	-	0		0
	Rapid City	24	43	3	8	0	0	0		0
	Williston	27	32	7	10	0	T	T	(S)	0
10/23	Aberdeen	35	46	10	4	0	0	0		0
	Bismark	36	43	10	3	0	0	0		0
	Fargo	34	39	10	10	0	0	0		0
	Huron	32	46	3	5	0	0	0		0
	Miles City	23	37	1	0	-	-	0		0
	Rapid City	29	42	0	0	0	0	0		0
	Williston	27	40	10	0	0	0	0		0
10/24	Aberdeen	31	54	0	4	0	0	0		0
	Bismark	33	48	0	7	0	0	0		0
	Fargo	33	49	0	8	0	0	0		0
	Huron	36	57	0	1	0	0	0		0
	Miles City	35	44	5	10	-	-	0		0
	Rapid City	36	57	0	3	0	0	0		0
	Williston	30	42	5	7	0	0	T		0
10/25	Aberdeen	38	37	10	10	0	0	0		0
	Bismark	34	39	10	10	0	0	0		0
	Fargo	38	42	10	10	0	0	0		0
	Huron	43	40	8	10	0	0	0		0
	Miles City	33	44	10	10	-	-	T		0
	Rapid City	34	54	1	1	0	0	0		0
	Williston	30	42	10	10	T	0	T		0
10/26	Aberdeen	46	56	0	4	0	0	0		0
	Bismark	41	57	3	10	0	0	0		0
	Fargo	43	53	0	7	0	0	0		0
	Huron	46	61	0	0	0	0	0		0
	Miles City	44	52	0	10	-	-	T		0
	Rapid City	53	65	0	5	0	0	0		0
	Williston	39	50	6	10	0	0	T	(R)	0

TABLE 3

Year 1984	Site	Air Temp (°F)		Cloud Cover (x/10)		Precip. (in.)				Snow Pack (in.)
		00	12	00	12	00	12	24h	Rem	24h
12/2	Aberdeen	17	10	10	4	T	0	T	(S)	2
	Bismark	14	19	10	10	T	T	.01	(S)	1
	Fargo	8	3	10	10	T	T	T	(S)	T
	Huron	19	14	10	1	.01	T	.07	(S)	6
	Miles City	13	11	10	9	.	.	.01	(S)	4
	Rapid City	19	19	4	4	0	0	T	(S)	T
	Williston	11	8	10	8	T	0	T	(S)	1
12/3	Aberdeen	4	17	0	4	0	0	T	(S)	2
	Bismark	15	15	10	7	T	T	T	(S)	1
	Fargo	0	10	0	0	0	T	0.1		T
	Huron	5	14	0	0	0	0		T(S)	6
	Miles City	-3	-2	10	1	.	.	0		4
	Rapid City	11	27	0	1	0	0	0		T
	Williston	9	9	10	8	T	T	T	(S)	1
12/4	Aberdeen	13	10	10	0	0	0	0.02	(S)	2
	Bismark	8	15	10	1	T	0	T		1
	Fargo	9	15	10	0	0	0	0		T
	Huron	5	12	6	2	T	0	T	(S)	5
	Miles City	-1	7	0	10	.	.	0		4
	Rapid City	15	24	2	0	0	0	0		T
	Williston	-5	10	0	10	0	0	0		1
12/5	Aberdeen	14	7	3	5	T	0	T	(S)	2
	Bismark	19	-1	4	0	0	0	T	(S)	1
	Fargo	11	-1	10	10	0	0	T	(S)	T
	Huron	15	15	4	7	0	T	T		4
	Miles City	24	13	10	10	.	.	T	(S)	3
	Rapid City	26	19	8	7	0	T	T	(S)	T
	Williston	8	-5	3	3	T	0	T	(S)	1
12/6	Aberdeen	-14	3	0	0	0	0	0		2
	Bismark	-11	20	0	8	0	0	T		1
	Fargo	-8	8	0	3	0	0	0		T
	Huron	-6	11	0	4	0	0	0		4
	Miles City	9	23	0	9	.	.	0		3
	Rapid City	6	44	1	1	0	0	0		T
	Williston	-7	24	0	9	0	0	T		1
12/7	Aberdeen	18	42	7	4	0	0	0		2
	Bismark	30	43	9	8	0	0	0		1
	Fargo	12	43	7	9	0	0	0		T
	Huron	19	42	3	0	0	0	0		3
	Miles City	35	44	4	0	.	.	0		2
	Rapid City	43	61	10	0	0	0	0		0
	Williston	34	43	3	6	0	0	0		1
12/8	Aberdeen	30	36	2	3	0	0	0		T
	Bismark	31	42	7	2	0	0	0		T
	Fargo	30	43	2	5	0	0	0		0
	Huron	31	42	0	4	0	0	0		1
	Miles City	29	33	3	3	.	.	0		1
	Rapid City	33	51	0	10	0	0	0		0
	Williston	31	37	7	8	0	0	0		T
12/9	Aberdeen	-	46	-	7	0	0	0		T
	Bismark	31	43	2	3	0	0	0		T
	Fargo	29	40	0	9	0	0	0		0
	Huron	35	39	7	7	0	0	0		T
	Miles City	26	35	5	4	.	.	0		1
	Rapid City	43	58	6	0	0	0	0		0
	Williston	28	37	0	2	0	0	0		0
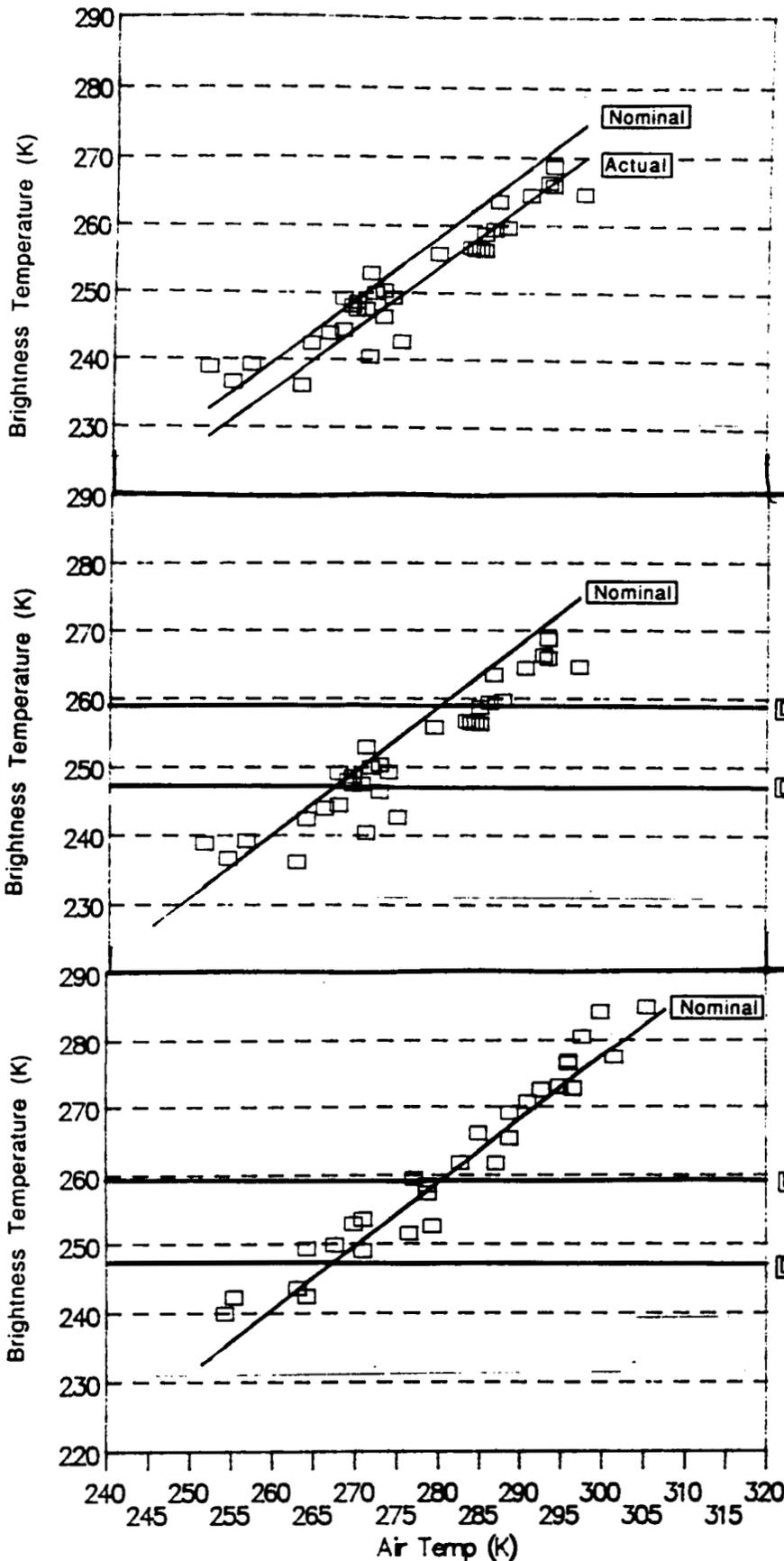
(a) <u>Midnight</u>. A linear regression of the Bismark data is shown ("Actual" curve), with a regression line for data collected throughout North Dakota and the surrounding region ("Nominal" curve).

(b) <u>Midnight</u>. Shown with the Bismark data is a linear regression for data collected throughout North Dakota and the surrounding region ("Nominal" curve). Also shown are brightness temperature decision thresholds for a frozen or thawed surface.

(c) <u>Noon</u>. Shown with the Bismark data is a linear regression for data collected throughout North Dakota and the surrounding region ("Nominal" curve). Also shown are brightness temperature decision thresholds for a frozen or thawed surface.

<u>Figure 1</u>.   37 GHz SMMR brightness temperature versus measured surface air temperature, Bismark, North Dakota. Data were collected from 8/1/84 to 12/31/84.
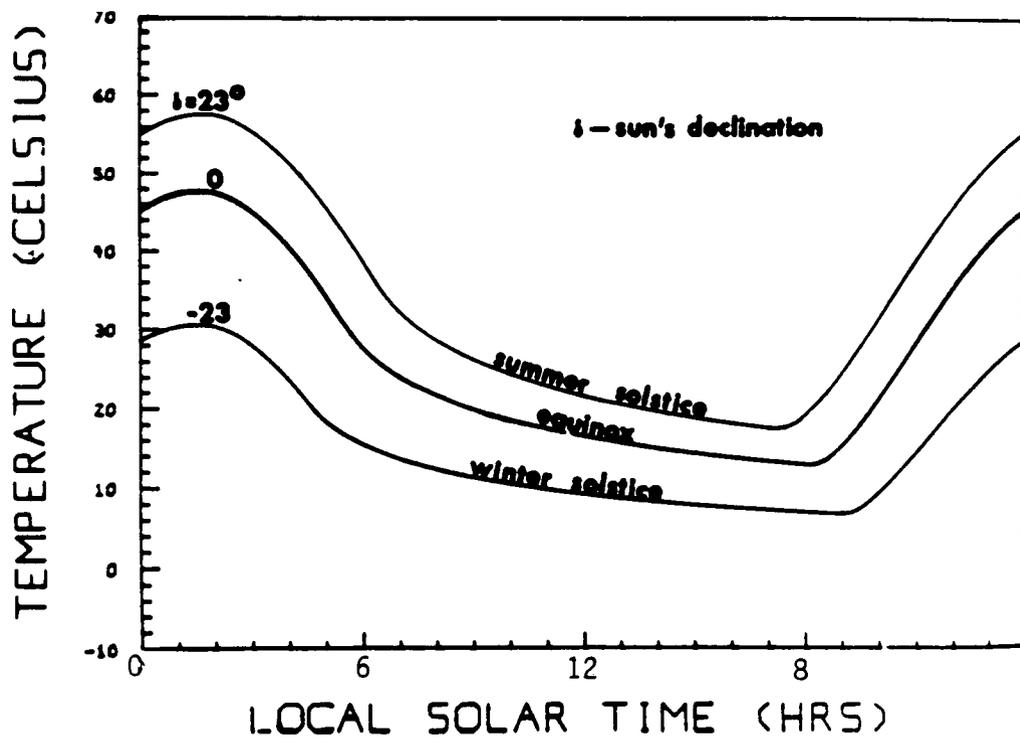
Figure 2. Diurnal surface temperature variation for different seasons at 30° N (from Watson, et al., 1983). Subsurface temperatures will exhibit a reduced amplitude and a phase lag with respect to the surface temperature. That is, midnight thermal gradients will be negative, and noon thermal gradients will be positive.

(a) Midnight

(b) Noon
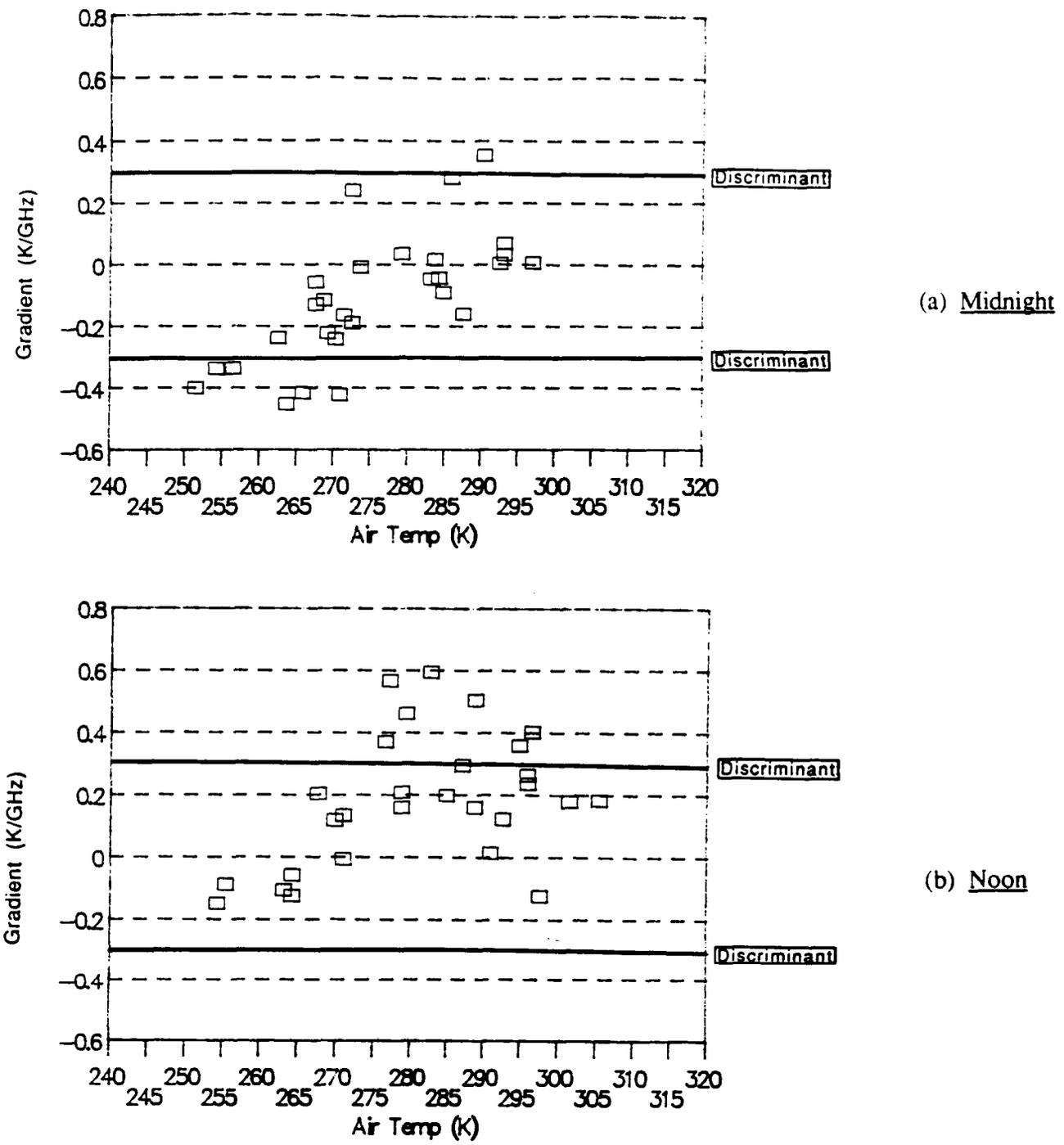
Figure 3. Frequency gradient versus measured surface air temperature, Bismark, North Dakota. Data were collected from 8/1/84 to 12/31/84. The frequency gradient is the frequency regression slope for simultaneous SMMR brightness temperatures at 37GHz, 18 GHz, and 10.7 GHz. Shown with the Bismark data are frequency gradient decision thresholds for a frozen or thawed surface.
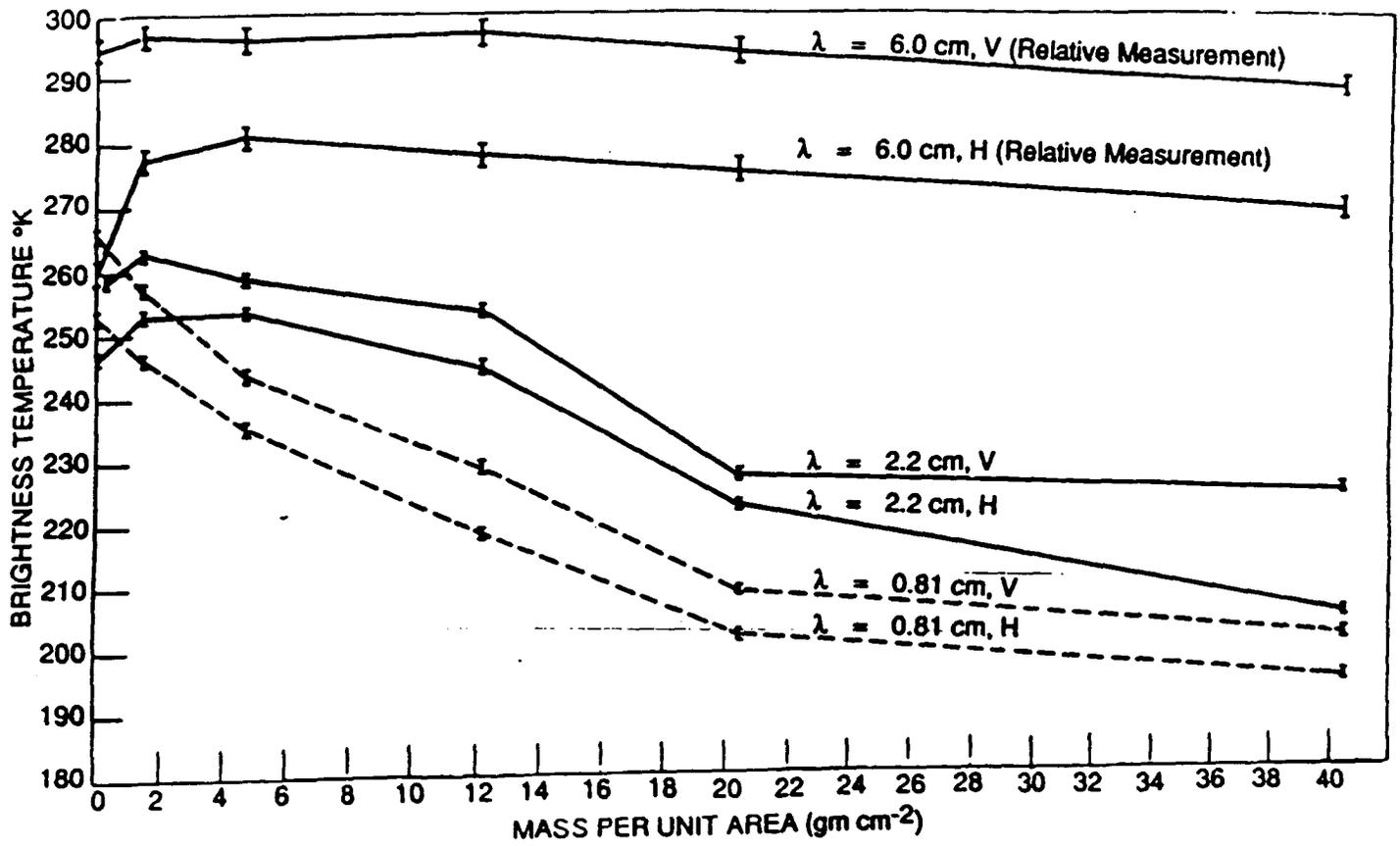
Figure 4. Brightness temperature versus equivalent dry snow, Crater Lake, Oregon, 22 March 1970 (Edgerton et al., 1971). Note the short wavelength darkening evident for thick snowpacks.
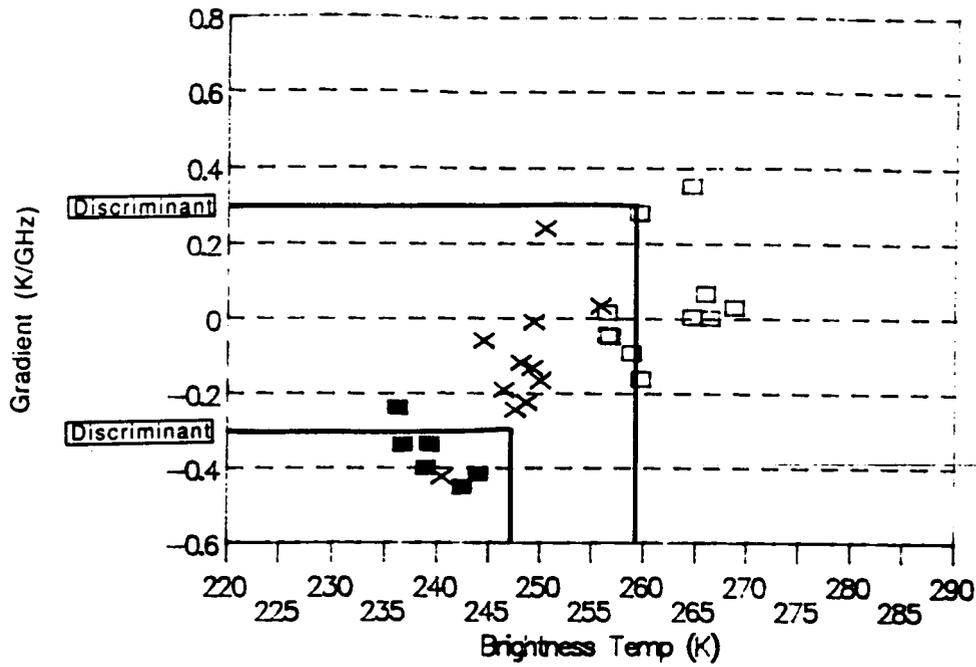
(a) Midnight
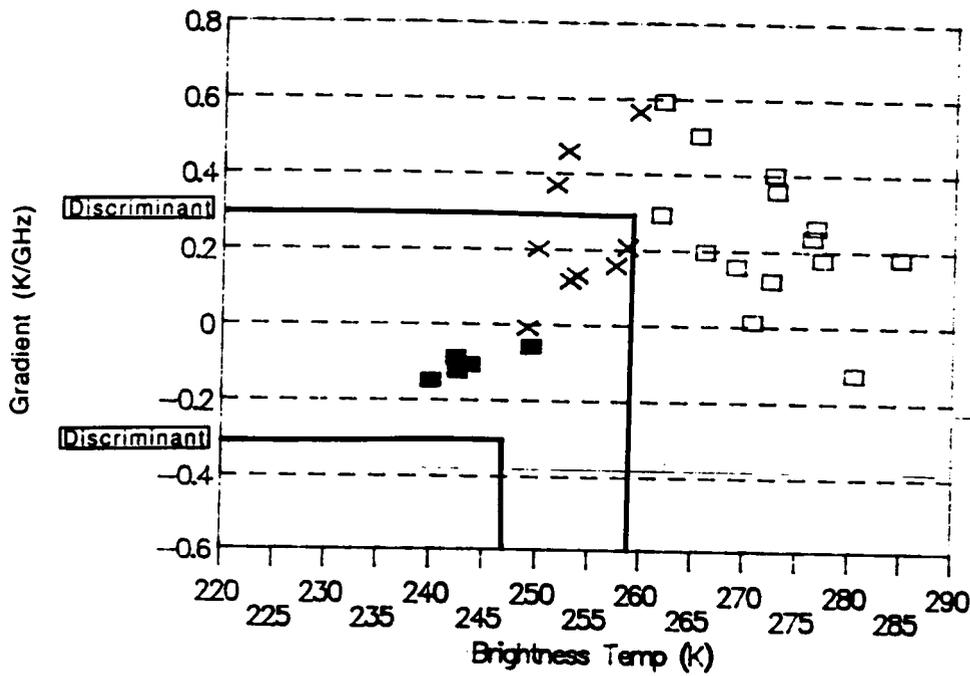
(b) Noon

Figure 5. Frequency gradient versus SMMR 37 GHz brightness temperature, Bismark, North Dakota. Data were collected from 8/1/84 to 12/31/84. Shown with the Bismark data are clustering decision thresholds for a frozen, mixed, or thawed surface. Based upon ground truth, the solid boxes are frozen, open boxes are thawed, and x's are mixed pixels.

(a) Midnight

(b) Noon
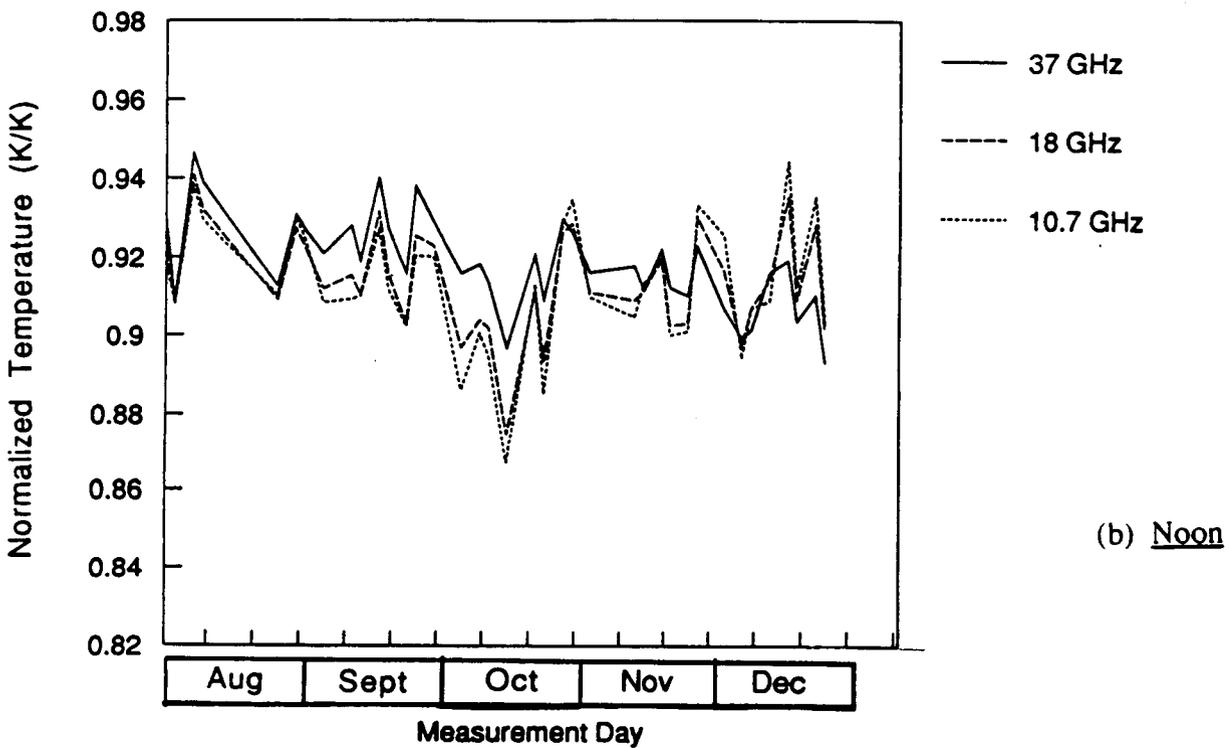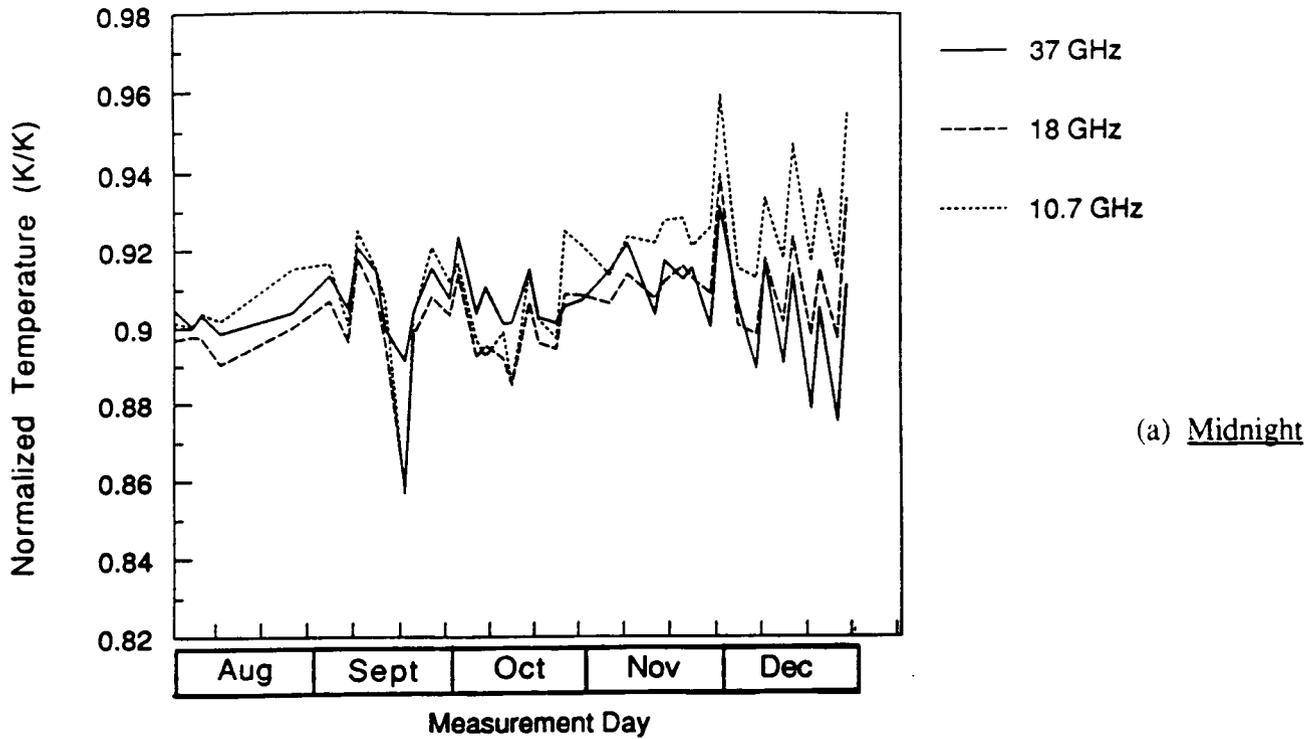
Figure 6.   37 GHz, 18 GHz, and 10.7 GHz SMMR normalized brightness temperatures versus calender day.   Measurements were made at irregular intervals from 8/1/84 to 12/31/84. The normalized brightness temperature of a single SMMR frequency channel is the average brightness divided by the average surface air temperature, averages are calculated over North Dakota and the surrounding region.

Air and Ground Temp   Night 9/20/84

AIR TEMP

Thaw ○
Mixed ⊗
Freeze ●

GND TEMP

Thaw □
Mixed ▨
Freeze ■
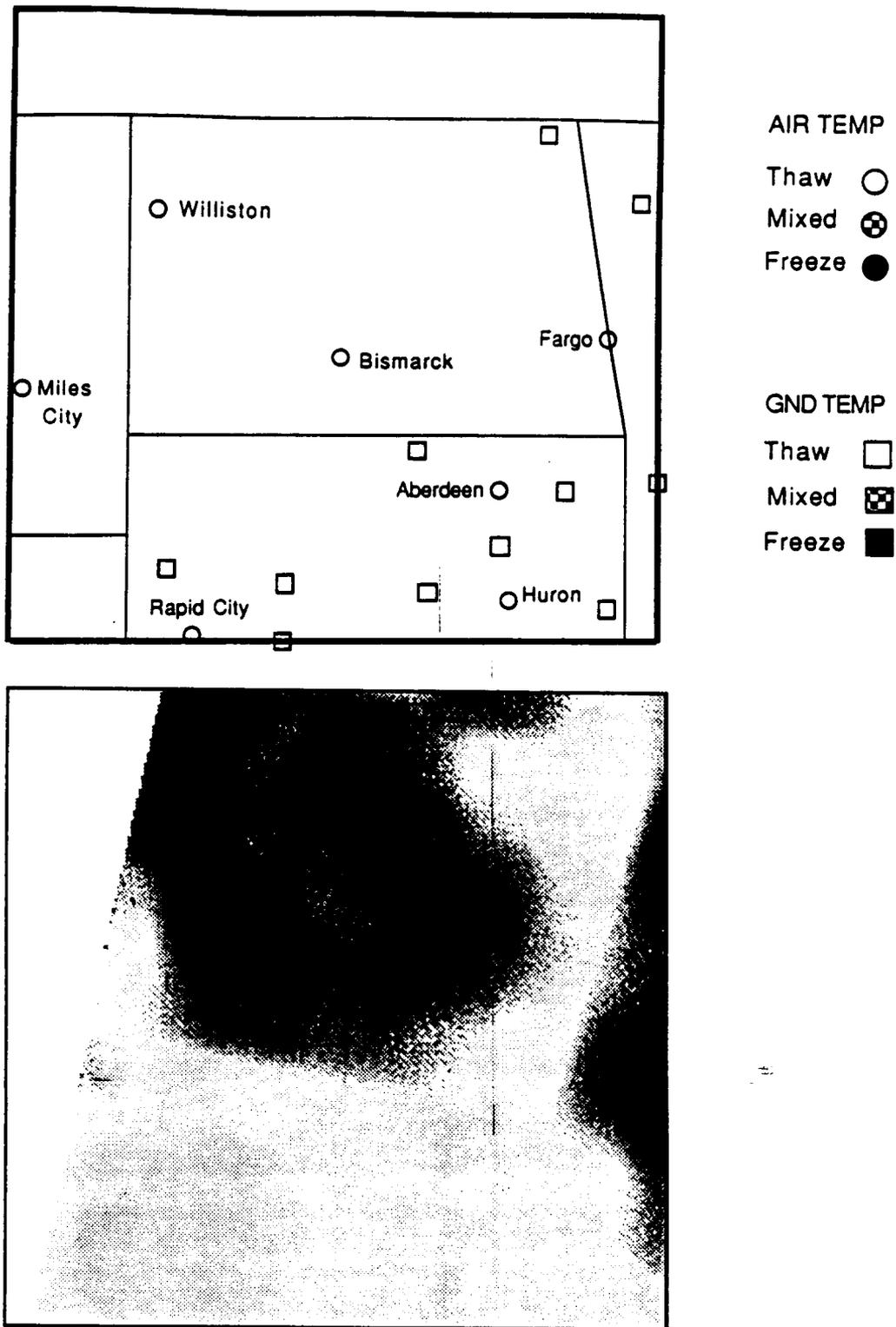
Figure 7.   A comparison of reported air and ground temperatures with the Freeze Indicator for midnight, September 20, 1984.

Air and Ground Temp   Night 10/24/84

AIR TEMP

Thaw ○
Mixed ◉
Freeze ●

GND TEMP

Thaw □
Mixed ▨
Freeze ■

Williston

Miles City

Bismarck

Fargo

Aberdeen

Rapid City

Huron
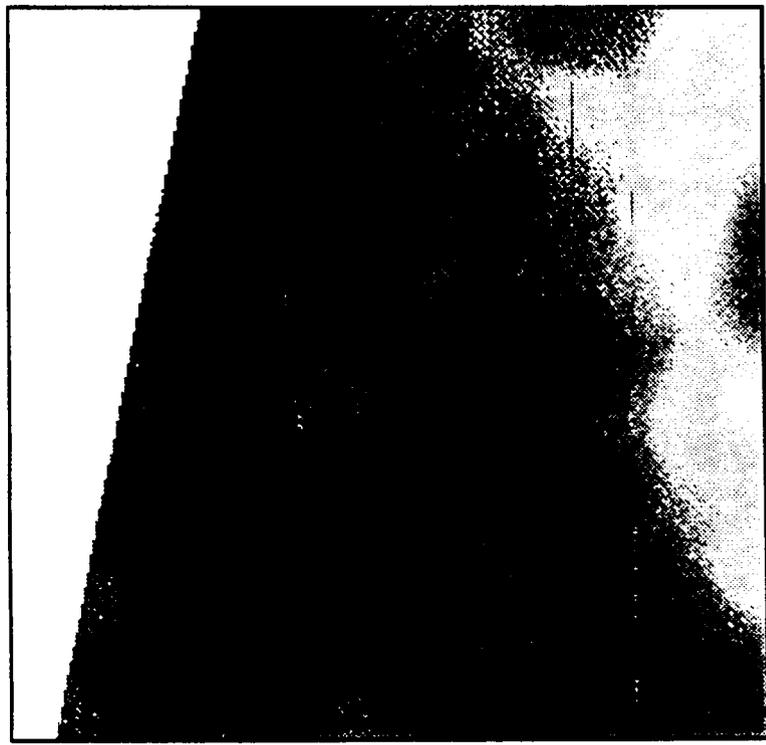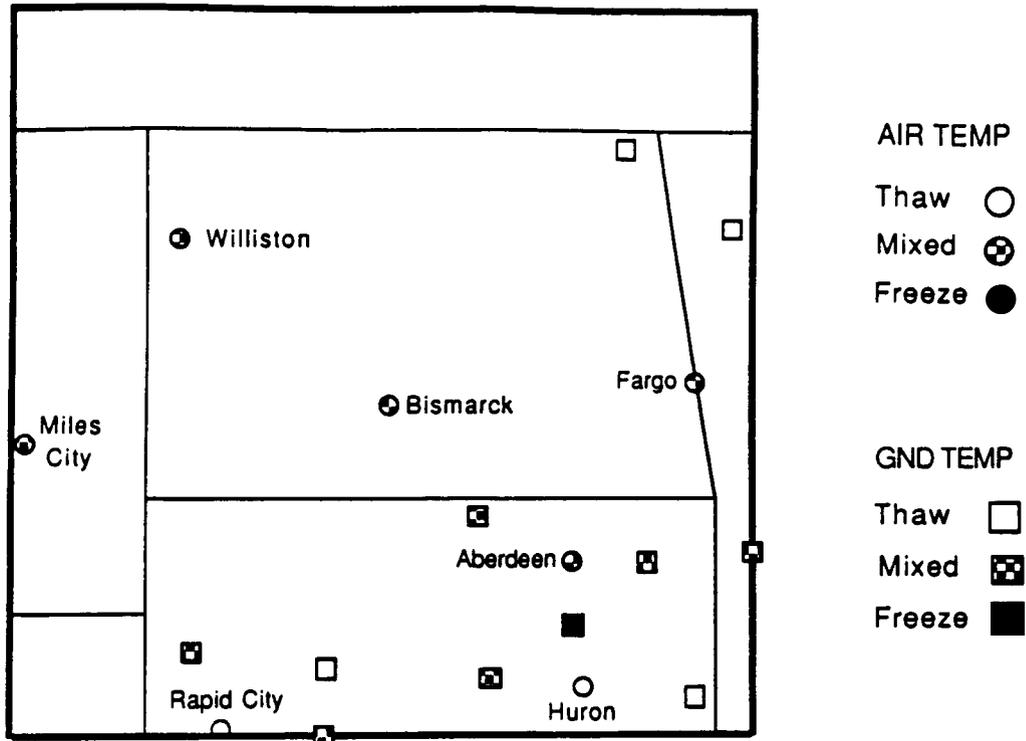
Figure 8.   A comparison of reported air and ground temperatures with the Freeze Indicator for midnight, October 24, 1984.

Air and Ground Temp   Night 12/9/84

AIR TEMP

Thaw ○
Mixed ⊕
Freeze ●

GND TEMP

Thaw □
Mixed ▥
Freeze ■

Williston

Miles City

Bismarck

Fargo

Rapid City

Huron
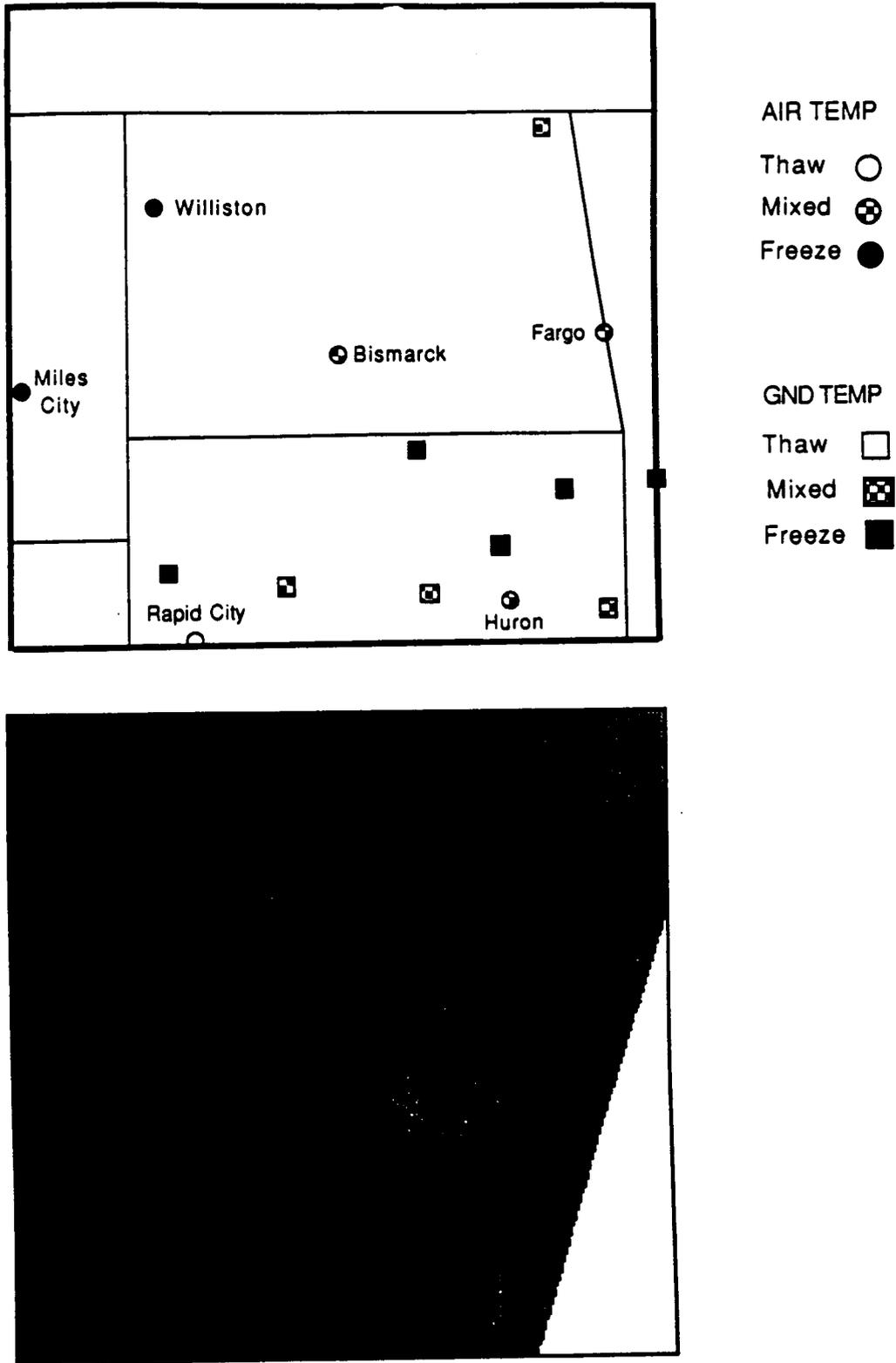
Figure 9.   A comparison of reported air and ground temperatures with the Freeze Indicator for midnight, December 9, 1984.

37 GHZ RADIOBRIGHTNESS   MIDNIGHT   FREEZE INDICATOR
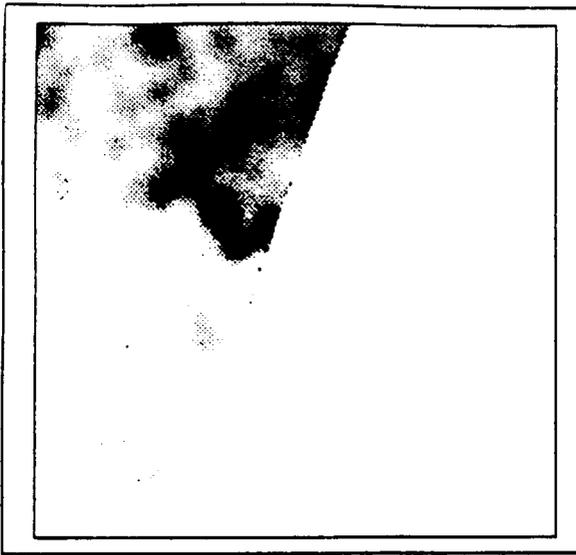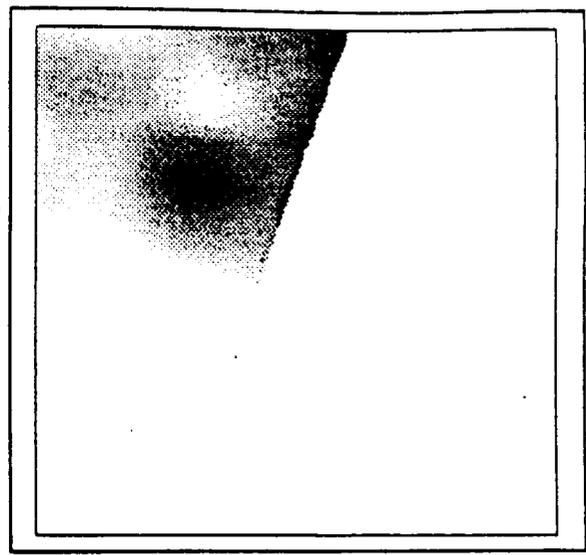
(9/16/84)

AN047S5   AN047FG

(9/18/84)
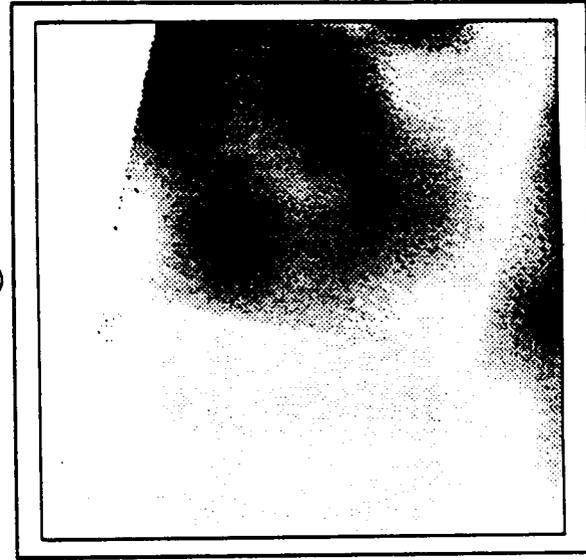
(9/20/84)

AN051S5   AN051FG

(9/22/84)
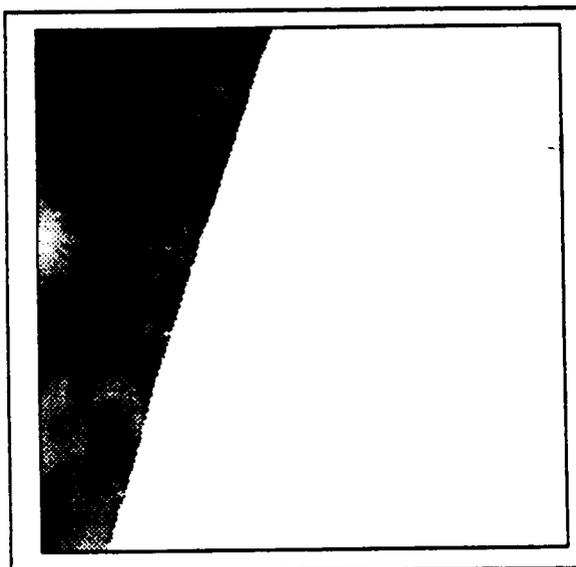
AN053S5   AN053FG
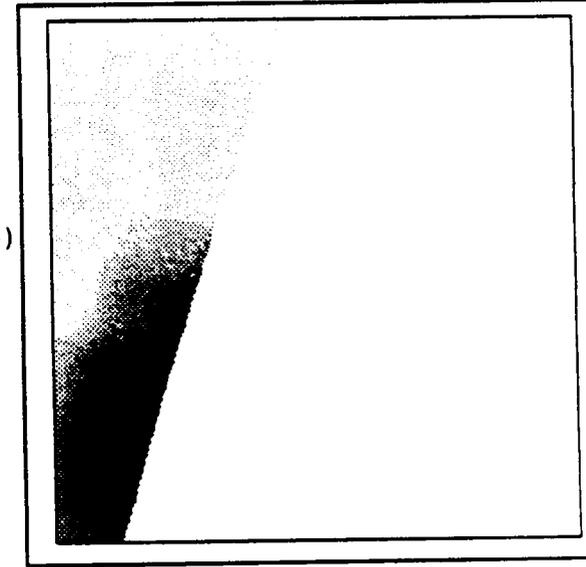
Figure 10(a).   Midnight 37 GHz and Freeze Indicator image sequences for a 6 day period in September.

37 GHZ RADIOBRIGHTNESS   NOON   FREEZE INDICATOR

(9/16/84)

AD047S5   AD047FG

(9/18/84)

AD049S5   AD049FG

(9/20/84)

(9/22/84)

AD053S5   AD053FG
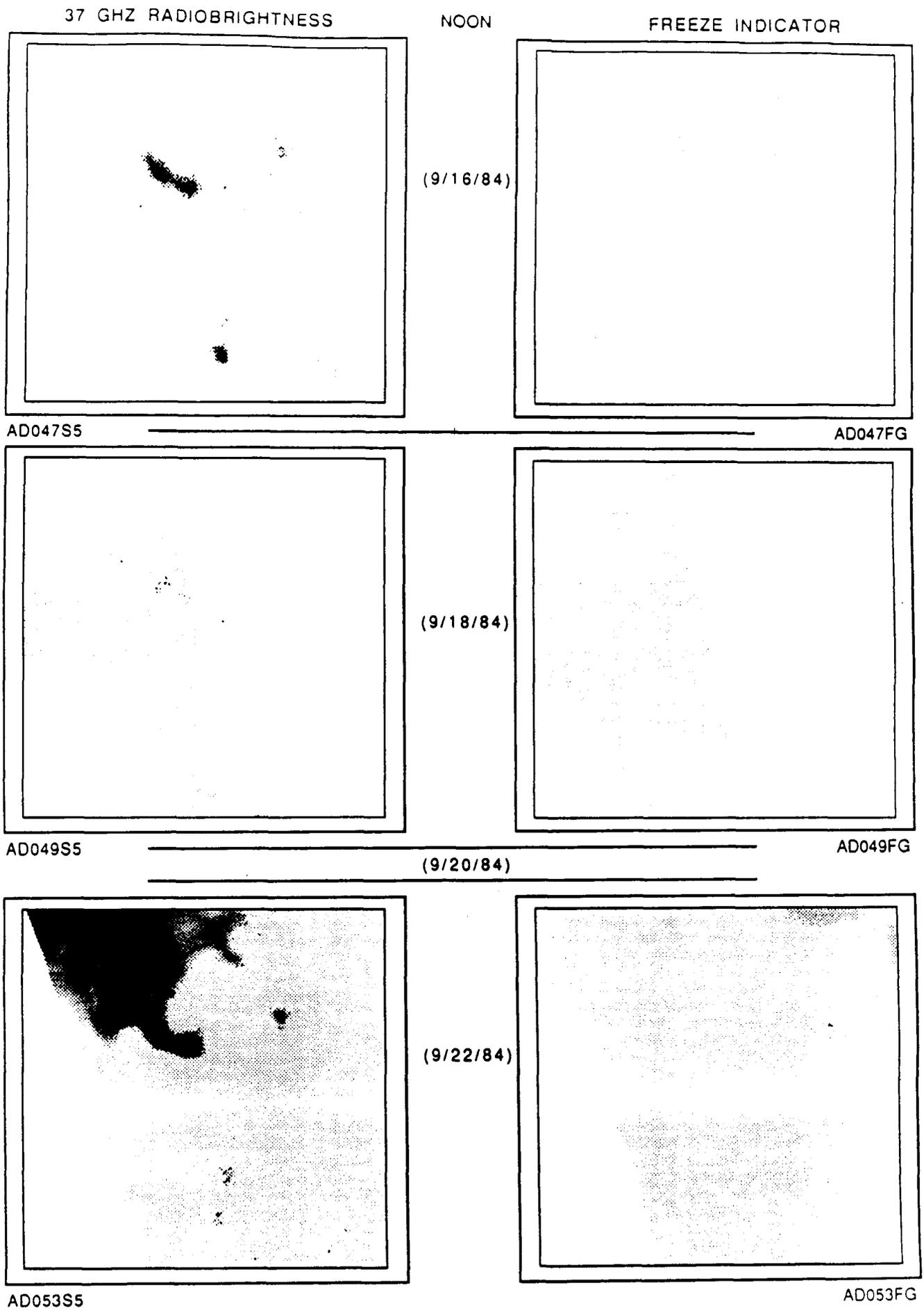
Figure 10(b).   Noon   37 GHz and Freeze Indicator image sequences for a 6 day period in
September.

37 GHZ RADIOBRIGHTNESS **MIDNIGHT** **FREEZE INDICATOR**

(10/20/84)

AN081S5

(10/22/84)

(10/24/84)

AN081FG

AN085S5

AN085FG

(10/26/84)

AN087S5

AN087FG
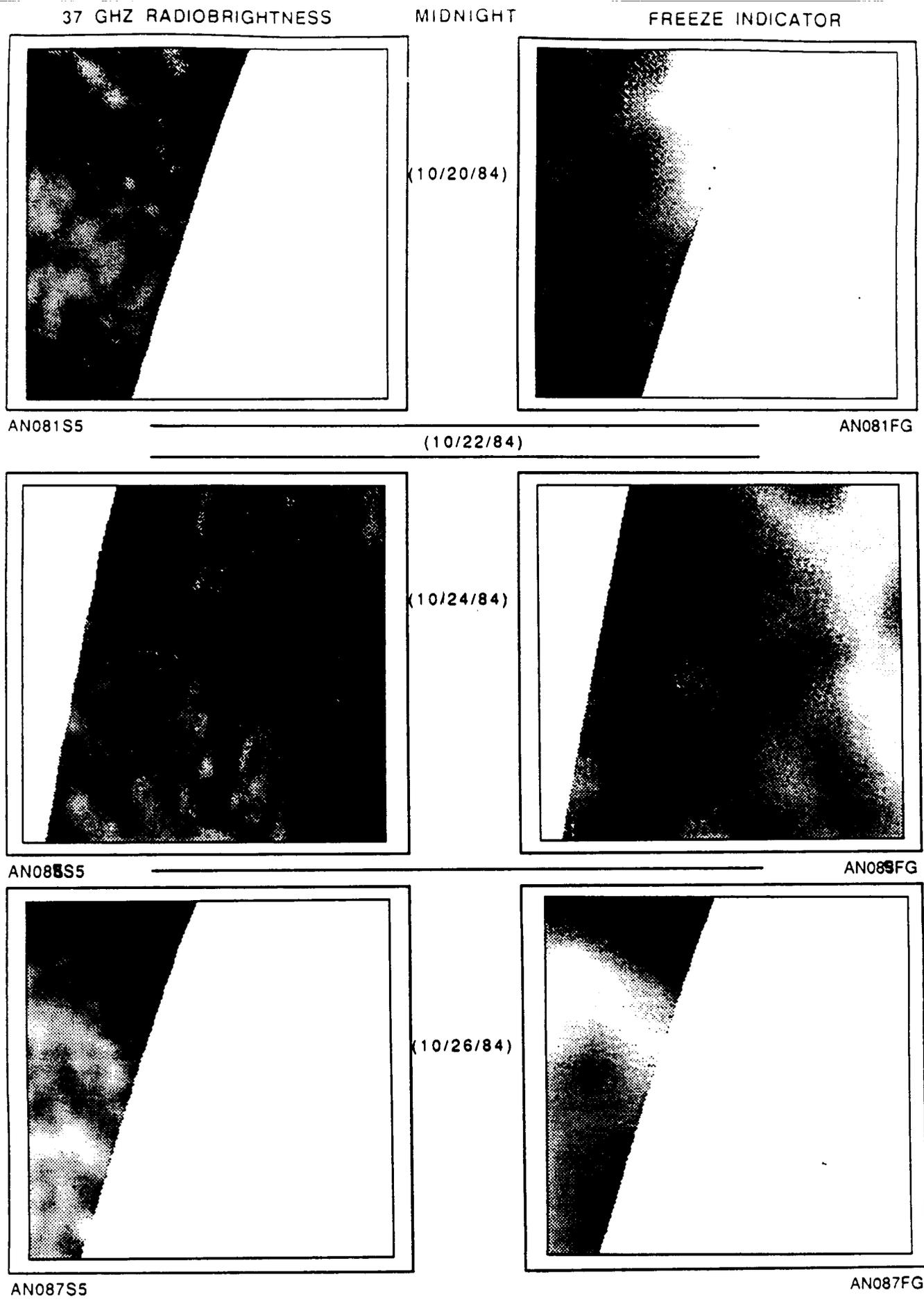
Figure 11(a). Midnight 37 GHz and Freeze Indicator image sequences for a 6 day period in October.

37 GHZ RADIOBRIGHTNESS   NOON   FREEZE INDICATOR

(10/20/84)
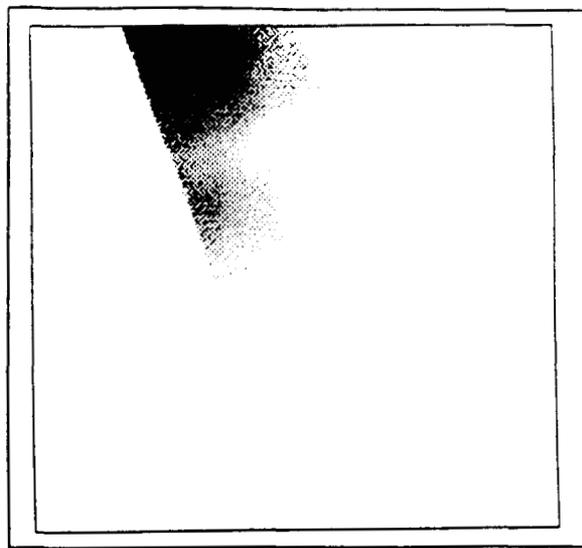
AD081S5   AD081FG
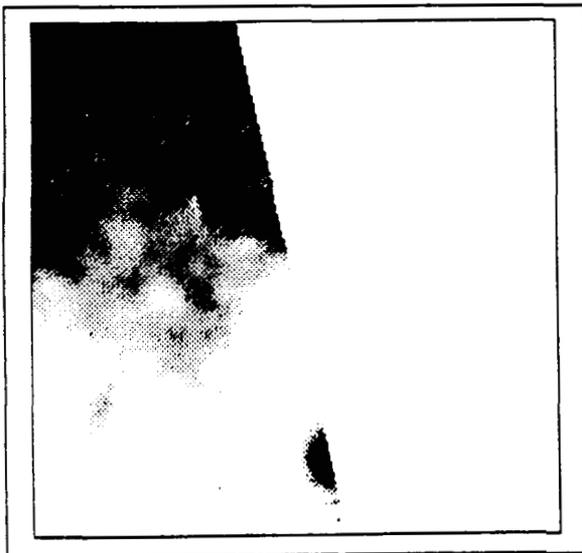
(10/22/84)
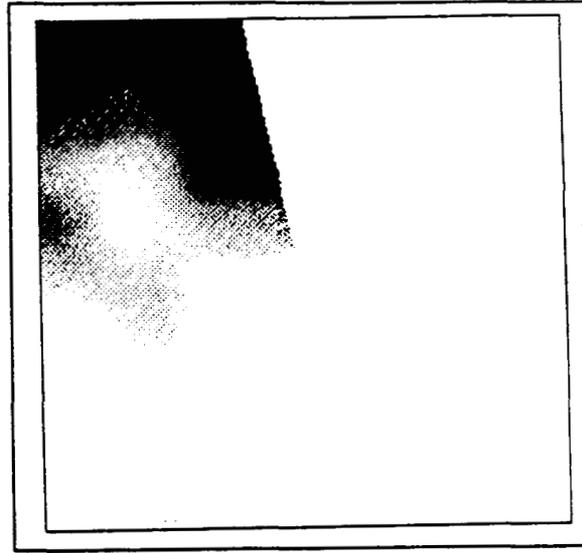
AD083S5   AD083FG

(10/24/84)

(10/26/84)
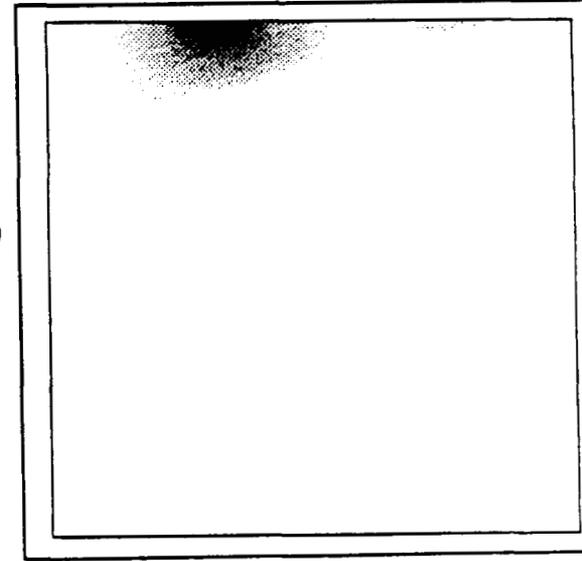
AD087S5   AD087FG

Figure 11(b).   Noon   37 GHz and Freeze Indicator image sequences for a 6 day period in October.

37 GHZ RADIOBRIGHTNESS   MIDNIGHT   FREEZE INDICATOR

(12/3/84)

AN125S5   AN125FG

(12/5/84)

AN127S5   AN127FG

AN129S5   (12/7/84)   AN129FG

(12/9/84)

AN131S5   AN131FG
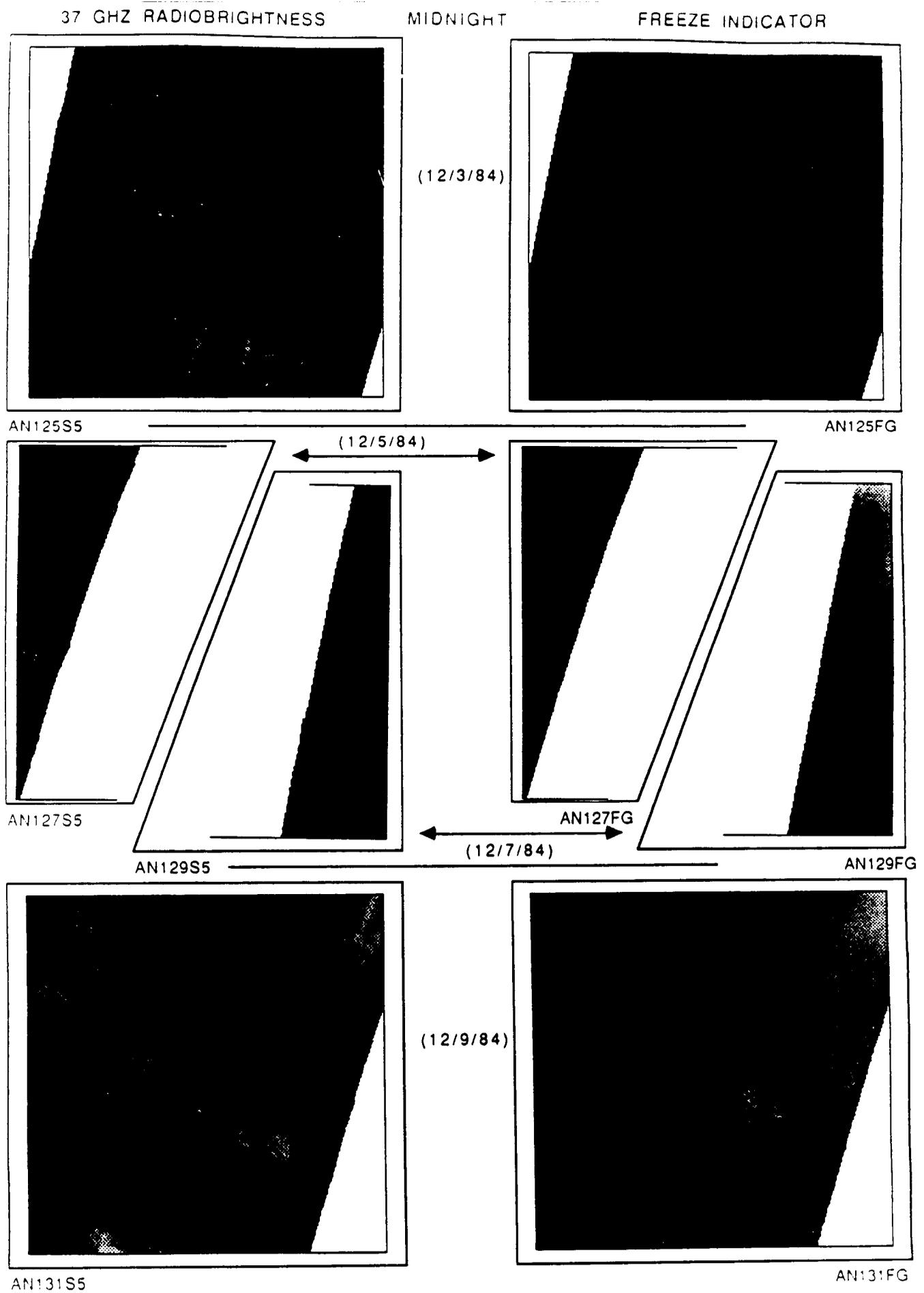
Figure 12(a).   Midnight 37 GHz and Freeze Indicator image sequences for a 6 day period in December.

(12/3/84)
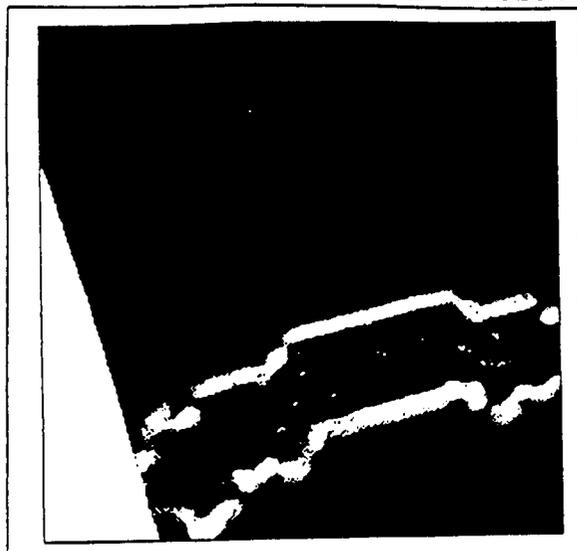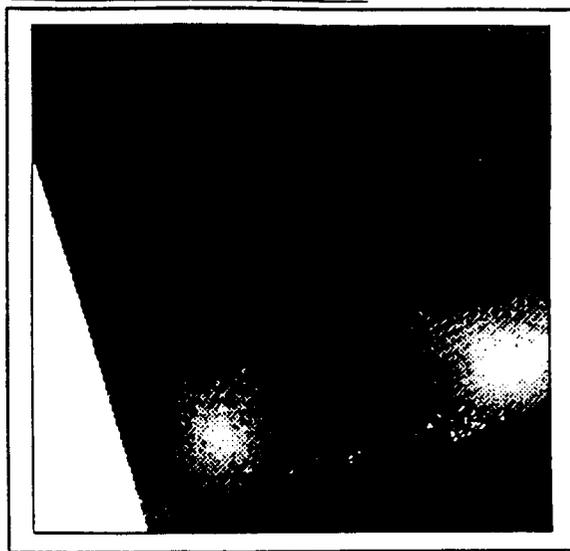
(12/5/84)

AD127S5   AD127FG

(12/7/84)
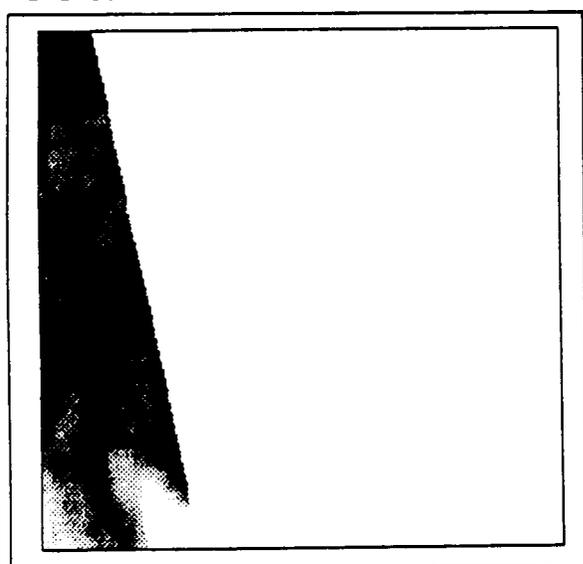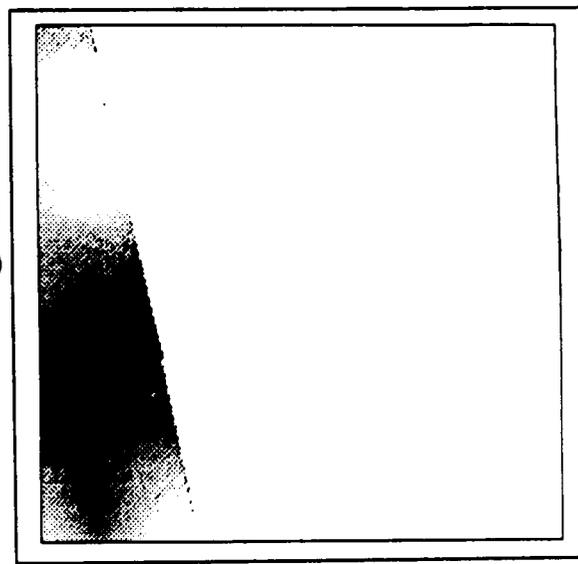
AD129S5   AD129FG

(12/9/84)
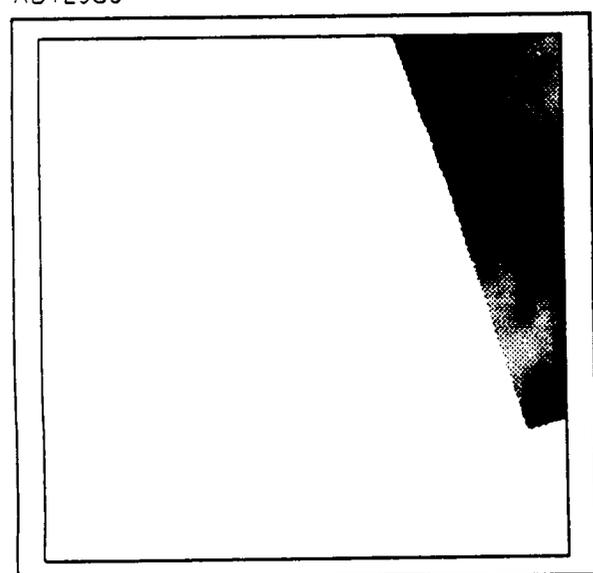
AD131S5   AD131FG
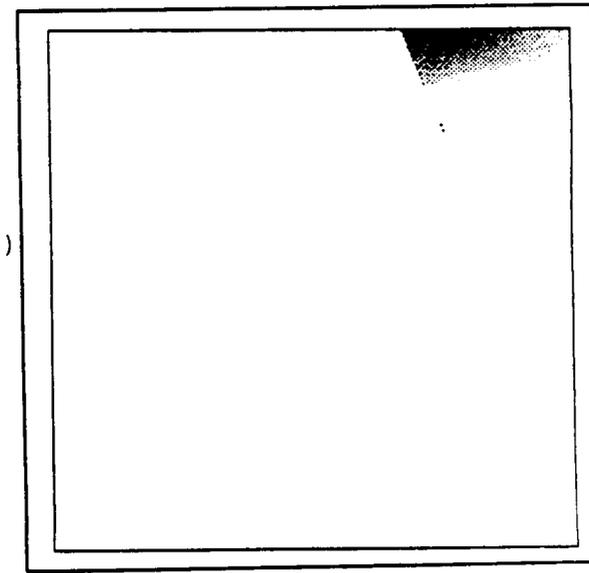
Figure 12(b).   Noon 37 GHz and Freeze Indicator image sequences for a 6 day period in
December. The jagged white lines in the Noon, 12/5/84, image are caused by
missing data.